Local protein synthesis in axon terminals and dendritic spines differentiates plasticity contexts

One sentence summary: Protein synthesis occurs in all synaptic compartments, including excitatory and inhibitory axon terminals.

Anne-Sophie Hafner[1,*], Paul G. Donlin-Asp[1,*], Beulah Leitch[2], Etienne Herzog[3,4], Erin M. Schuman[1#]

1: Max Planck Institute for Brain Research, Frankfurt Germany
2: Department of Anatomy, Otago School of Biomedical Sciences, University of Otago, Dunedin, New Zealand
3: Interdisciplinary Institute for Neuroscience, University Bordeaux, UMR 5297, F-33000, Bordeaux, France.
4: Interdisciplinary Institute for Neuroscience, CNRS, UMR 5297, F-33000, Bordeaux, France.

* Authors contributed equally to this work

To whom correspondence should be addressed: erin.schuman@brain.mpg.de

Abstract.

While there is ample evidence for localized mRNAs and protein synthesis in mature neuronal postsynaptic compartments, clear demonstrations of these processes in presynaptic terminals are extremely limited. Using expansion microscopy to resolve pre- and postsynaptic compartments we discovered that most presynaptic terminals contain mRNA and ribosomes. Using fluorescence-activated synaptosome sorting, we directly visualized or sequenced hundreds of mRNA species within excitatory boutons. Following brief metabolic labeling, over 30% of all presynaptic terminals exhibit a signal, providing evidence for ongoing protein synthesis. Using different classic plasticity paradigms, we discovered unique patterns of rapid pre- and/or postsynaptic translation. These data suggest that local protein synthesis in both pre- and postsynaptic elements is differentially recruited to drive the unique compartment-specific phenotypes that underlie different forms of plasticity.

Main text.

The complement of proteins present at neuronal synapses represents the best phenotypic indicator of both the type and strength of the synapse. The regulation of synaptic proteins, by post-translational modifications and by ongoing protein synthesis and degradation, drives homeostasis and plasticity at synapses (*1-3*). Due to the compartmentalized nature of neurons, where axons and dendrites are remote from the cell body, there is a certain attractiveness to proposals that a substantial fraction of proteomic remodeling occurs locally within both axons and dendrites (*4-6*). While there is wealth of data indicating that protein synthesis occurs in mature dendrites (*6, 7*) there has been much less evidence in support of local translation in mature axons, due to early failures to detect ribosomes within the axon (*8*). Nevertheless, many studies have shown that local translation is required for axonal development and repair (e.g. (*9-12*)). In addition, a few recent studies have shown that mature axons contain competent translational machinery and mRNAs (*13*) or use presynaptic translation during plasticity (*14*).

Efforts to localize molecules or cell biological events to neuronal pre- or postsynaptic compartments using fluorescence microscopy have been limited by the tight association of the axonal bouton and the dendritic spine or synapse; the synaptic cleft, the only clear region of separation, is just ~ 20 nm wide. Here, in order to increase the resolving power to visualize mRNA molecules in pre- and postsynaptic compartments, we optimized fluorescence in situ hybridization (FISH) and nascent protein detection methods for use with expansion microscopy (*15*) (Fig. 1A; see Methods). Using cultured rat hippocampal neurons (DIV 18-21), we found that expansion resulted in a clear enlargement of both pre- and postsynaptic compartments, with an average expansion of ~3.5 fold (fig. S1), yielding a clear separation between the pre- and postsynaptic compartments (Supplemental video 1). To detect all mature mRNA species, we used a poly d(T) FISH probes to detect polyadenylated mRNA in neurons transfected with the fluorescent protein mCherry to visualize their morphology (fig. S2). Poly(A) mRNA was abundant in both dendrites and thin axonal processes (fig. S3). In order to quantify the incidence of poly(A) contained in presynaptic terminals, we combined poly(A) FISH with immunolabelling for either excitatory (vGLUT1+;(*16, 17*)) or inhibitory (vGAT+;(*18, 19*)) nerve terminals in expanded cultured hippocampal

neurons. We detected poly(A) mRNA in 82% and 83% percent of excitatory and inhibitory presynaptic nerve terminals, respectively (Fig. 1B-E; fig. S4). We also detected signal outside of the immunolabeled compartment which reflects mRNA present in other (unlabeled) cells and compartments that has been cross-linked to the gel (fig. S3); RNAse treatment dramatically reduced all signal (fig. S5). To examine whether the cellular machinery for protein translation is present, we probed for ribosomal RNA (rRNA) and ribosomal protein RPS11. We detected ribosomes in a large majority of both excitatory and inhibitory presynaptic nerve terminals, using RPS11 immunostaining (fig. S5-7) and *in situ* hybridization against 28S rRNA (Fig. 1B-E). Taken together, these data indicate an abundance of mRNAs and ribosomes in unambiguously identified excitatory and inhibitory presynaptic nerve terminals.

The presence of poly(A) mRNA in axon terminals suggests the capacity for protein synthesis, but does not indicate the breadth of translational machinery or the mRNA population potentially available for translation in identified synapse types. In order to capture the full complement of presynaptic transcripts in excitatory presynaptic terminals, we turned to our recently developed platform that couples fluorescence-sorting with biochemical fractionation to purify fluorescently labelled synaptosomes (fluorescence-activated synaptosome sorting; FASS) comprising resealed presynaptic synaptic compartments, sometimes associated with an “open” postsynaptic membrane (*20-22*). Starting with the forebrain of adult vGLUT1^{venus} knock-in mice in which all vGLUT1+ synapses are fluorescently labeled (*23*), we prepared synaptosomes and sorted vGLUT1+ synaptosomes for FISH, immunocytochemisry and RNA sequencing (Fig. 1F; fig. S8-9). We first examined whether the vGLUT1+ sorted synaptosome population, reflecting excitatory synaptic composition *in vivo*, possess some of the molecular elements that we previously detected in the expanded cultured hippocampal synapses (Fig. 1 B-E). Using sparse plating of individual vGLUT1+ synaptosomes combined with confocal imaging we determined the incidence of poly(A) mRNA and ribosomal proteins together with a postsynaptic density marker protein, PSD-95 (Fig. 1F-L). We found that over 80% of all sorted vGLUT1+ synaptosomes contained poly(A) mRNA and ribosomal protein; a smaller fraction (~65%) were associated with PSD-95 (Fig. 1H,K). Using the pre-sorted synaptosome population (which contains both excitatory and inhibitory synapses) we labeled either excitatory (vGLUT1+) or inhibitory (vGAT+) synaptosomes and, similarly, found that over 80% of all presynaptic

compartments contain ribosomal proteins (fig. S10) indicating that both excitatory and inhibitory terminals contain translation machinery. We took advantage of the punctate nature of the imaged fluorescent signals to calculate the center-to-center distances for the three proteins. The distances we measured are consistent with the localization of PSD-95 in the postsynaptic compartment, with its' closest neighbor as vGLUT1, present across the synaptic cleft in the presynaptic terminal (mean distance 22 nm) (data not shown). Slightly offset from the cleft in the presynaptic terminal were poly(A) mRNA and RPS11 (Fig. 1I, 1L), suggesting the possibility that presynaptic translation occurs in relatively peripheral regions within terminals, not directly at the active zone. Note that theopen (not-sealed) nature of the postsynaptic compartment in this synaptosome preparation prevented us from detecting/analyzing the incidence poly(A) mRNA and RPS11 in this compartment. Using STED microscopy we confirmed the tight spatial relationship between vGLUT1 and RPS11 (Fig. 1M). These data indicate that a large majority of the presynaptic terminals, both excitatory and inhibitory, contain both polyA mRNA and ribosomal protein, indicating the capacity for protein synthesis.

To discover the ensemble of transcripts present in adult mouse synapses, we used RNA sequencing to identify the mRNA population of both the pre-sorted and vGLUT1^{+} synaptosomes (see Methods). From 2 biological replicates, we obtained 147 Mio reads that, following genome alignment, yielded 4172 transcripts detected in both replicates and in both conditions (117 Mio uniquely mapped reads in total) (fig. S11). Because the vGLUT+ sorted population is a subsample of the pre-sorted synaptosome sample, we expected and indeed obtained a large (86.9%) overlap in transcript identity (Fig. 2A; fig. S11) and a minor overlap with prior synaptic sequencing studies (fig. S11). Amongst the transcripts uniquely detected in the pre-sorted sample there was an over representation of transcripts coding for endoplasmic reticulum and Golgi apparatus related proteins (Fig. 2B), consistent with the de-enrichment of potential contaminants (fig. S9). In the list of transcripts uniquely detected in vGLUT1+ sorted synaptosomes we detected proteins involved in lipid raft assembly (Fig. 2C). This suggests, as previously described, an important role for lipid rafts in regulating presynaptic function (*24*). A functional analysis of the 4172 transcripts identified in both pre-sorted and vGLUT1+ sorted synaptosomes revealed that transcripts coding for proteins associated with presynaptic function were among the most enriched including neurotransmitter uptake, synaptic vesicle exocytosis and transport (Fig. 2D). In order

to isolate specifically the local transcriptome in vGLUT1+ excitatory terminals available for local proteome remodeling, we undertook a differential gene expression approach and compared the abundance of mRNA transcripts in the pre-sorted to vGLUT1+ sorted synaptosomes. We identified 156 transcripts that were significantly enriched in sorted synaptosome and gene ontology analysis revealed an over representation of genes coding for ribosomal proteins and regulator of translation (Fig2 E). Amongst the most (> 1.2-fold) enriched in the vGLUT1^{+} presynaptic transcriptome we noted the presence of many well-known mRNAs coding presynaptic proteins including *Bassoon* (Bsn), *Rims1* and *Rims3*, as well as signaling molecules like *Sergef* and the ryanodine receptor (*Ryr3*) (Fig. 2G-I). Amongst the 264 transcripts depleted in the vGLUT1+ synaptosome transcriptome were many transcripts coding for postsynaptic proteins such as neurotransmitter receptors of the GABA and AMPA family, indicating the depletion of postsynaptic and dendritic components through our synaptosome sorting (Fig. 2 F). Also, transcripts coding well-known endoplasmic reticulum marker proteins, including *Ergic1*, *Calr* or *Sec62*, were diminished in the vGLUT1+ sorted synaptosomes (Fig. 2H). Using multiple synaptic annotation databases (Table S2), we identified many previously annotated synaptic transcripts associated with a variety of cellular functions (Fig. 2I). We validated the presence of several of the enriched transcripts including *Rapgef4*, *Adcy1*, *Bsn*, and *Kif5a* in sparsely plated vGLUT1+ synaptosomes using single molecule FISH (Fig. 2J-L & Fig. S11). These data indicate that presynaptic compartments from adult mouse forebrain contain the requisite machinery and an ample mRNA population for protein synthesis.

To obtain direct evidence for protein synthesis in synaptic compartments, particularly presynaptic boutons, we adapted the puromycin-based metabolic labeling strategy (*25*) for detection using electron microscopy. Cultured hippocampal neurons were briefly (10 min) labelled with puromycin and then fixed and processed for electron microscopy (EM) using immunogold labeling with an anti-puromycin antibody (see Methods). Using transmission electron microscopy, we were able to identify, based on morphological features (see Methods), both dendrites and synapses in the EM images (Fig. 3A). We found that the inclusion of the protein synthesis inhibitor anisomycin or the omission of puromycin, led to a dramatic reduction in the detected gold particles (Fig. 3A-C; fig. S12). We found that the majority of presynaptic boutons and postsynaptic spines contained puromycin-positive gold particles indicating active

protein synthesis within the last 10 minutes (Fig. 3B-C). The thin nature of the EM sections precludes a 3D analysis and may result in an under-estimation of the level of ongoing protein synthesis in pre- and postsynaptic compartments. To address the frequency of translation in a well-resolved 3D volume of both presynaptic boutons and dendritic spines we used metabolic labeling in expanded cultured hippocampal neurons (Fig. 3D). Together with 5 min of metabolic labeling of nascent protein synthesis, we conducted immunocytochemical analyses using pre- (vGLUT1+ or vGAT, excitatory or inhibitory) and postsynaptic mCherry expression. By analyzing the coincidence of the synaptic markers with the metabolic label, we conclude that an average of ~37 and 61% percent of excitatory pre- and postsynaptic compartments, respectively, underwent active translation in a 5 min window, while ~44% of inhibitory presynaptic terminals underwent translation; the omission of the metabolic label or the addition of the protein synthesis inhibitor anisomycin resulted in dramatically reduced signal (fig. S13). Furthermore, we validated the local translation of some specific candidate mRNAs, identified in the presynaptic transcriptome (Fig. 2E), using Puro-PLA (*26*) together with immunolabeling to identify postsynaptic and pre-synaptic compartments (anti-Map2 and vGLUT1 antibodies, respectively). With just 5 minutes of metabolic labeling, we visualized, for example, the new synthesis of both RapGEF4 and Bassoon in presynaptic compartments (Fig. 3F-G). Taken together, these data indicate that postsynaptic spines as well as excitatory and inhibitory presynaptic boutons exhibit local translation with a relatively high frequency, in the absence of any exogenous stimulation.

Local translation is required for several forms of synaptic plasticity including, but not limited to, potentiation induced by neurotrophins (*27*), and depression induced by metabotropic glutamate receptor activation$_{1/5}$ (mGluR$_{1/5}$) (*28*) or endocannabinoids (*14*). Capitalizing on our ability to visualize the protein synthesis that occurs in three different synaptic compartments (the dendritic spine and both excitatory and inhibitory presynaptic boutons), we examined the translational signature of these three different forms of plasticity. We treated cultured hippocampal neurons with brain-derived neurotrophic factor (BDNF), an mGluR$_{1/5}$ agonist ((S)-3,5-Dihydroxyphenylglycine hydrate; DHPG) or an endocannabinoid CB1 receptor agonist (arachidonyl-2-chloroethylamide; ACEA), adding a metabolic label for the last 5 minutes of each treatment (Fig. 4A). Immunocytochemical detection of nascent protein and markers of

each compartment was conducted and the samples were then subjected to expansion microscopy. We evaluated the pattern of protein synthesis in the three compartments of interest and found that each type of plasticity yielded a different constellation of translation loci: BDNF caused an increase in local translation in dendritic spines and both excitatory and inhibitory boutons (Fig. 4B-E), DHPG caused an increase in dendritic spines only, and ACEA caused an increase in inhibitory boutons exclusively (Fig. 4C-E); addition of anisomycin significantly reduced the signal in all conditions (fig. S13). In separate experiments, we examined whether the above three agonists bring about changes in the frequency or amount of poly(A) mRNA and found no significant change (fig. S14). These data indicate that the compartment-specific translation observed above is mediated by enhanced protein synthesis of mRNAs already resident at the synapse.

Here, we investigated the localization and stimulation of protein synthesis in mature synapses, with unprecedented spatial resolution, allowing us to visualize protein synthesis machinery and translation in individual pre- and postsynaptic compartments. We found that over 80% of dendritic spines and both excitatory and inhibitory presynaptic terminals contain rRNA, ribosomes and poly(A) mRNA. We show with both light (confocal and super-resolution) and electron microscopy that in the absence of overt stimulation, there is a surprisingly high level of ongoing protein synthesis in both pre- and postsynaptic compartments: with just 5 min of labeling ~40% of both excitatory and inhibitory presynaptic terminals and ~ 60% of dendritic spines exhibit active translation. Puromycin, a tRNA mimic, was used to metabolically label nascent proteins (*25*); we used an optimized low concentration in order to label nascent peptides while avoiding a complete block of protein synthesis. As such, we believe that the above estimates represent a conservative “lower-bound” of the fraction of compartments undergoing translation in the labeling window.

We and others have previously demonstrated thousands of mRNA transcripts are present distally in neuronal processes, where they can be locally used for protein synthesis (*29-32*). Notably, the transcriptome of retinal ganglion cell axons has been characterized both during development (*33, 34*) and the retinal ganglion cell translatome has been identified in the adult mouse (*13*). Here, using mouse forebrain synaptosomes that are enriched for “intact” presynaptic terminals we identified a large

(~4300) local transcriptome available for translation during basal and plastic conditions. Within this transcriptome, we detected many transcripts that code for proteins that regulate vesicle release probability including *Rims*, *Adcy1*, and *Bsn*. Using Puro-PLA (*26*) we directly detected the synthesis of several presynaptic proteins, including RapGEF and Bassoon, in identified nerve terminals within minutes of metabolic labeling. These data suggest that local translation of presynaptic proteins may work in concert with the well-documented transport of presynaptic proteins and complexes within axons to supply and regulate neurotransmitter release and homeostasis in individual, mature, healthy nerve terminals.

Multiple forms of synaptic plasticity involve local translation in dendrites including, BDNF-induced synaptic potentiation (*27*), mGluR-dependent long-term depression (*35*), dopamine-induced plasticity (*36*) and homeostatic plasticity (*37*) and activation of presynaptic CB1 receptors by retrograde endocannabinoid signaling stimulates local protein synthesis in inhibitory terminals to produce long-term depression of inhibitory transmission (*14*). We found local translation in both the pre- and postsynaptic compartments is differentially regulated by 3 of the above forms of plasticity in a compartment-specific manner. These data indicate that there is also information about the recent synaptic history and the expression of plasticity in the particular pattern of translation loci in synaptic compartments. Together with the selection of particular mRNAs for translation, owing to unique regulatory elements present in the 3'UTRs (*38*), a unique and remodeled synaptic proteome for each kind of plasticity can be achieved. Taken together, our findings demonstrate that local protein synthesis is a ubiquitous feature of brain synapses- it occurs in dendritic spines, excitatory and inhibitory presynaptic boutons under basal conditions and is differentially recruited in these compartments to modify local proteomes.

References and Notes.

1. A. R. Dorrbaum, L. Kochen, J. D. Langer, E. M. Schuman, Local and global influences on protein turnover in neurons and glia. *Elife* **7**, (2018).
2. C. T. Schanzenbacher, S. Sambandan, J. D. Langer, E. M. Schuman, Nascent Proteome Remodeling following Homeostatic Scaling at Hippocampal Synapses. *Neuron* **92**, 358-371 (2016).
3. C. Hanus, E. M. Schuman, Proteostasis in complex dendrites. *Nat Rev Neurosci* **14**, 638-648 (2013).
4. K. C. Martin, A. Ephrussi, mRNA localization: gene expression in the spatial dimension. *Cell* **136**, 719-730 (2009).
5. S. J. Van Driesche, K. C. Martin, New frontiers in RNA transport and local translation in neurons. *Dev Neurobiol* **78**, 331-339 (2018).
6. C. Glock, M. Heumuller, E. M. Schuman, mRNA transport & local translation in neurons. *Curr Opin Neurobiol* **45**, 169-177 (2017).
7. C. E. Holt, E. M. Schuman, The central dogma decentralized: new perspectives on RNA function and local translation in neurons. *Neuron* **80**, 648-657 (2013).
8. R. J. Lasek, C. Dabrowski, R. Nordlander, Analysis of axoplasmic RNA from invertebrate giant axons. *Nat New Biol* **244**, 162-165 (1973).
9. D. S. Campbell, C. E. Holt, Chemotropic responses of retinal growth cones mediated by rapid local protein synthesis and degradation. *Neuron* **32**, 1013-1026 (2001).
10. C. J. Donnelly, M. Fainzilber, J. L. Twiss, Subcellular communication through RNA transport and localized protein synthesis. *Traffic* **11**, 1498-1505 (2010).
11. K. M. Leung, F. P. van Horck, A. C. Lin, R. Allison, N. Standart, C. E. Holt, Asymmetrical beta-actin mRNA translation in growth cones mediates attractive turning to netrin-1. *Nat Neurosci* **9**, 1247-1256 (2006).
12. D. E. Willis, E. A. van Niekerk, Y. Sasaki, M. Mesngon, T. T. Merianda, G. G. Williams, M. Kendall, D. S. Smith, G. J. Bassell, J. L. Twiss, Extracellular stimuli specifically regulate localized levels of individual neuronal mRNAs. *J Cell Biol* **178**, 965-980 (2007).
13. T. Shigeoka, H. Jung, J. Jung, B. Turner-Bridger, J. Ohk, J. Q. Lin, P. S. Amieux, C. E. Holt, Dynamic Axonal Translation in Developing and Mature Visual Circuits. *Cell* **166**, 181-192 (2016).
14. T. J. Younts, H. R. Monday, B. Dudok, M. E. Klein, B. A. Jordan, I. Katona, P. E. Castillo, Presynaptic Protein Synthesis Is Required for Long-Term Plasticity of GABA Release. *Neuron* **92**, 479-492 (2016).
15. P. W. Tillberg, F. Chen, K. D. Piatkevich, Y. Zhao, C. C. Yu, B. P. English, L. Gao, A. Martorell, H. J. Suk, F. Yoshida, E. M. DeGennaro, D. H. Roossien, G. Gong, U. Seneviratne, S. R. Tannenbaum, R. Desimone, D. Cai, E. S. Boyden, Protein-retention expansion microscopy of cells and tissues labeled using standard fluorescent proteins and antibodies. *Nat Biotechnol* **34**, 987-992 (2016).
16. E. Herzog, G. C. Bellenchi, C. Gras, V. Bernard, P. Ravassard, C. Bedet, B. Gasnier, B. Giros, S. El Mestikawy, The existence of a second vesicular glutamate transporter specifies subpopulations of glutamatergic neurons. *J Neurosci* **21**, RC181 (2001).
17. R. T. Fremeau, Jr., M. D. Troyer, I. Pahner, G. O. Nygaard, C. H. Tran, R. J. Reimer, E. E. Bellocchio, D. Fortin, J. Storm-Mathisen, R. H. Edwards, The

expression of vesicular glutamate transporters defines two classes of excitatory synapse. *Neuron* **31**, 247-260 (2001).
18. S. L. McIntire, R. J. Reimer, K. Schuske, R. H. Edwards, E. M. Jorgensen, Identification and characterization of the vesicular GABA transporter. *Nature* **389**, 870-876 (1997).
19. C. Sagne, S. El Mestikawy, M. F. Isambert, M. Hamon, J. P. Henry, B. Giros, B. Gasnier, Cloning of a functional vesicular GABA and glycine transporter by screening of genome databases. *Febs Lett* **417**, 177-183 (1997).
20. E. Luquet, C. Biesemann, A. Munier, E. Herzog, Purification of Synaptosome Populations Using Fluorescence-Activated Synaptosome Sorting. *Methods Mol Biol* **1538**, 121-134 (2017).
21. C. Biesemann, M. Gronborg, E. Luquet, S. P. Wichert, V. Bernard, S. R. Bungers, B. Cooper, F. Varoqueaux, L. Li, J. A. Byrne, H. Urlaub, O. Jahn, N. Brose, E. Herzog, Proteomic screening of glutamatergic mouse brain synaptosomes isolated by fluorescence activated sorting. *EMBO J* **33**, 157-170 (2014).
22. V. P. Whittaker, I. A. Michaelson, R. J. Kirkland, The separation of synaptic vesicles from nerve-ending particles ('synaptosomes'). *Biochem J* **90**, 293-303 (1964).
23. E. Herzog, F. Nadrigny, K. Silm, C. Biesemann, I. Helling, T. Bersot, H. Steffens, R. Schwartzmann, U. V. Nagerl, S. El Mestikawy, J. Rhee, F. Kirchhoff, N. Brose, In vivo imaging of intersynaptic vesicle exchange using VGLUT1 Venus knock-in mice. *J Neurosci* **31**, 15544-15559 (2011).
24. C. Salaun, D. J. James, L. H. Chamberlain, Lipid rafts and the regulation of exocytosis. *Traffic* **5**, 255-264 (2004).
25. E. K. Schmidt, G. Clavarino, M. Ceppi, P. Pierre, SUnSET, a nonradioactive method to monitor protein synthesis. *Nat Methods* **6**, 275-277 (2009).
26. S. tom Dieck, L. Kochen, C. Hanus, M. Heumuller, I. Bartnik, B. Nassim-Assir, K. Merk, T. Mosler, S. Garg, S. Bunse, D. A. Tirrell, E. M. Schuman, Direct visualization of newly synthesized target proteins in situ. *Nat Methods* **12**, 411-414 (2015).
27. H. Kang, E. M. Schuman, A requirement for local protein synthesis in neurotrophin-induced hippocampal synaptic plasticity. *Science* **273**, 1402-1406 (1996).
28. K. M. Huber, J. C. Roder, M. F. Bear, Chemical induction of mGluR5- and protein synthesis--dependent long-term depression in hippocampal area CA1. *J Neurophysiol* **86**, 321-325 (2001).
29. J. Zhong, T. Zhang, L. M. Bloch, Dendritic mRNAs encode diversified functionalities in hippocampal pyramidal neurons. *BMC Neurosci* **7**, 17 (2006).
30. E. S. Lein, M. J. Hawrylycz, N. Ao, M. Ayres, A. Bensinger, A. Bernard, A. F. Boe, M. S. Boguski, K. S. Brockway, E. J. Byrnes, L. Chen, *et al.,* Genome-wide atlas of gene expression in the adult mouse brain. *Nature* **445**, 168-176 (2007).
31. M. M. Poon, S. H. Choi, C. A. Jamieson, D. H. Geschwind, K. C. Martin, Identification of process-localized mRNAs from cultured rodent hippocampal neurons. *J Neurosci* **26**, 13390-13399 (2006).
32. I. J. Cajigas, G. Tushev, T. J. Will, S. tom Dieck, N. Fuerst, E. M. Schuman, The local transcriptome in the synaptic neuropil revealed by deep sequencing and high-resolution imaging. *Neuron* **74**, 453-466 (2012).
33. L. F. Gumy, G. S. Yeo, Y. C. Tung, K. H. Zivraj, D. Willis, G. Coppola, B. Y. Lam, J. L. Twiss, C. E. Holt, J. W. Fawcett, Transcriptome analysis of

embryonic and adult sensory axons reveals changes in mRNA repertoire localization. *RNA* **17**, 85-98 (2011).
34. K. H. Zivraj, Y. C. Tung, M. Piper, L. Gumy, J. W. Fawcett, G. S. Yeo, C. E. Holt, Subcellular profiling reveals distinct and developmentally regulated repertoire of growth cone mRNAs. *J Neurosci* **30**, 15464-15478 (2010).
35. K. M. Huber, M. S. Kayser, M. F. Bear, Role for rapid dendritic protein synthesis in hippocampal mGluR-dependent long-term depression. *Science* **288**, 1254-1257 (2000).
36. W. B. Smith, S. R. Starck, R. W. Roberts, E. M. Schuman, Dopaminergic stimulation of local protein synthesis enhances surface expression of GluR1 and synaptic transmission in hippocampal neurons. *Neuron* **45**, 765-779 (2005).
37. M. A. Sutton, H. T. Ito, P. Cressy, C. Kempf, J. C. Woo, E. M. Schuman, Miniature neurotransmission stabilizes synaptic function via tonic suppression of local dendritic protein synthesis. *Cell* **125**, 785-799 (2006).
38. G. Tushev, C. Glock, M. Heumuller, A. Biever, M. Jovanovic, E. M. Schuman, Alternative 3' UTRs Modify the Localization, Regulatory Potential, Stability, and Plasticity of mRNAs in Neuronal Compartments. *Neuron* **98**, 495-511 e496 (2018).

Acknowledgements.
We thank I. Bartnik, N. Fuerst, A. Staab and C. Thum for the preparation of cultured hippocampal neurons, S. tom Dieck and T.W. Lee for important work in preliminary studies, Ha Nguyen for experiments shown in Supplementary Figure S10, Maria Florencia Angelo for assistance with FASS experiments, Anaëlle Stum and Vincent Pitard for technical assistance (Flow cytometry facility, CNRS UMS 3427, INSERM US 005, Univ. Bordeaux, F-33000 Bordeaux, France), Fabrice Cordelières for image analysis routines (Bordeaux Imaging Center, Univ. Bordeaux, F-33000 Bordeaux, France) and Georgi Tushev for help with RNA sequencing analyses.
Funding: A.S.H. is supported by an EMBO Long-term Postdoctoral Fellowship (ALTF 1095-2015) and the Alexander von Humboldt Foundation (FRA-1184902-HFST-P) as well as France-BioImaging. P.G.D.A. is supported by the Peter and Traudl Engelhard Stiftung. E.M.S. is funded by the Max Planck Society, an Advanced Investigator award from the European Research Council, DFG CRC 1080: Molecular and Cellular Mechanisms of Neural Homeostasis and DFG CRC 902: Molecular Principles of RNA-based Regulation and the DFG Cluster of Excellence for Macromolecular Complexes, Goethe University. This project has received funding from the European Research Council (ERC) under the European Union's Horizon 2020 research and innovation program (grant agreement No 743216). B.L. is funded by the Royal Society NZ-Germany Science and Technology Programme FRG-UOO1403. E.H. is funded by the French Agence Nationale de la Recherche (ANR-10-LABX-43 BRAIN « Dolipran ») and the Fondation pour la Recherche Médicale (ING20150532192).
Author contributions: A.S.H. and P.D.A. designed, conducted and analyzed experiments. E.H. and B.L. designed and supervised experiments. E.M.S. designed experiments, supervised the project, and wrote the paper. All authors edited the paper.
Competing interests: The authors declare no competing financial interests.

Data and materials availability: all data is available in the manuscript or the supplementary materials.

List of Supplementary Materials.

Materials and Methods.

Table 1.

Figures S1-14.

References x-y.

Supplementary Video 1.

Figure Legends.

Fig. 1. Abundant ribosomes and mRNAs in both pre- and postsynaptic compartments of mature cultured hippocampal neurons.

(**A**) Scheme indicating the experimental flow: cultured neurons were processed for FISH and fluorescent immunostaining (IF; for presynaptic terminal types, excitatory VGLUT1+, inhibitory, VGAT+, or for a fluorescent marker protein) and then subjected to protein retention expansion microscopy protocol (see Methods). (**B**) Representative images of expanded pre-synaptic compartments chosen for their positive VGLUT1+ signal (magenta) showing the presence of both 28s RNA (green; top row) and poly (A) RNA (green; bottom row) detected with FISH as well as the merged images (last image in each trio). (**C**) Bar graph showing analysis for all VGLUT1+ compartments analyzed (n = 1213 and 1022 terminals from 8 different experimental dishes per condition) showing that over 80% of all VGLUT1+ terminals contain poly (A) RNA and 28s RNA. (**D**) Representative images of expanded pre-synaptic compartments chosen for their positive vGAT+ signal (magenta) showing the presence of both 28s RNA (green; top row) and poly (A) RNA (green; bottom row) as well as the merged images (last image in each trio). (**E**) Bar graph showing analysis for all vGAT+ compartments analyzed (n = 1240 and 1168 terminals from 8 different experimental dishes per condition) showing that over 80% of all vGAT+ terminals contain poly (A) RNA and 28s RNA. (**F**) Scheme showing experimental flow for analysis of the global (pre-sorted) synaptosome population as well as the analysis of fluorescently sorted vGLUT1+ synaptosomes which comprise for the most part closed pre-synaptic terminals, a smaller fraction of which have an associated postsynaptic density. (**G**) Representative confocal images of sparsely plated vGLUT1+ synaptosomes showing the positive vGLUT1 signal in each synaptosome panel as well as the presence or absence of poly(A) (top panels) of poly(U) (bottom panels) repeated RNA sequences or PSD-95 for the same samples. Merged images are shown in the last panel of images. (**H**) Bar graph showing analysis for all synaptosomes analyzed (including sorted and pre-sorted as the populations did not differ- see Methods) (n^{dT} = 921 and n^{dA} = 1069 terminals from 4 different experimental dishes) showing that ~87% of all VGLUT1+ terminals were positive for a FISH oligo-dT probe (indicating the presence of poly (A) RNA species) while less than ~18% were positive for a FISH oligo-dA probe. ** Unpaired t-test, $p \leq 0.01$. (**I**) Plot of all data points for sorted synaptosomes and median as well as scheme showing center-to-center distance of the various signals measured. The center of the oligo-dT

signal (green) is on average ~12 nm from the center of the vGLUT1 signal (lavender) and ~19 nm from the PSD-95 signal (black). (n^{vGLUT1} = 317 and n^{PSD-95} = 134) *** Unpaired t-test, $p \leq 0.001$. (**J**) Representative immunofluorescence and FISH images of sparsely plated vGLUT1+ synaptosomes showing the positive vGLUT1 signal in each synaptosome panel as well as the presence or absence of the ribosomal protein RPS11 or PSD-95 for the same samples. Merged images are shown in the last panel of images. (**K**) Bar graph showing analysis for all synaptosomes analyzed (n = 568 from 3 different experimental dishes) showing that greater than 80% of all vGLUT1+ terminals were positive for RPS11 and ~60% were positive for PSD-95. *** Unpaired t-test, $p \leq 0.001$. (**L**) Plot of merged data for pre-sorted and sorted synaptosomes and median as well as scheme showing center-to-center distance of the various signals measured. The center of the RPS11 signal (green) is on average ~13 nm from the center of the vGLUT1 signal (lavender) and ~19 nm from the PSD-95 signal (black). *** Unpaired t-test, $p \leq 0.001$. (**M**) Super-resolved (STED) images of a synaptosome particle showing the spatial relationship between the RPS11 and vGLUT1 signal. All scale bars = 5 μm. Error bars represent standard deviation (S.D.).

Fig. 2. An excitatory presynaptic transcriptome from mature mouse synapses.
(A) Venn diagram indicating the total number of transcripts identified (in 2/2 biological replicates) from RNA seq of pre-sorted and vGLUT1+ synaptosomes. (**B-C**) Gene Ontology (GO) annotations of transcripts exclusively detected in both replicates of y pre-sorted and vGLUT1+ sorted samples. (**D**) Extracted neuronal GO process annotations of the 10% most abundant transcripts (in RPM) from the overlapping population detected in pre- and vGLUT1+ sorted synaptosomes. (**E**) GO process annotations for the 156 transcripts significantly enriched in vGLUT1+ sorted samples corresponding to vGLUT1+ local transcriptome. (**F**) Examples of individual transcripts that are significantly enriched in the vGLUT1+ transcriptome. (**G**) GO process annotation for the 264 transcripts significantly de-enriched in vGLUT1+ sorted samples corresponding to transcripts that are most likely localized in non-synaptic compartment (**H**) Examples of individual transcripts that are significantly de-enriched in the vGLUT1+ transcriptome. (**I**) Table indicating the function of the 46 sorted sample transcripts that have been previously annotated as coding for synaptic proteins. (**J-K**) Fluorescence in situ hybridization (FISH) conducted on isolated vGLUT1+ synaptosomes validating the presence of *Rapgef4* and *Bsn* mRNA in vGLUT1+ terminals. (**L**). Analysis of FISH data

indicating the percentage of vGLUT1+ synaptosomes that possess the indicated mRNA. *** Kruskal-Wallis nonparametric test followed by Dunn's multiple comparison test, $p \leq 0.001$. All scale bars = 5 μm. Error bars represent S.D.

Fig. 3. In vivo isolated pre- and postsynaptic compartments actively translate protein in the absence of external stimulation.

(**A**) Electron microscope (EM) images of cultured hippocampal neurons metabolically labeled with puromycin for 10 min and then detected using immunogold (see Methods). Electron-dense particles indicate sites of protein synthesis. Shown are a dendritic segment (left) and a synapse (right) with gold particles present throughout the dendrite as well as in both the presynaptic (shaded lavender) and postsynaptic (shaded pale green) compartments. Yellow arrows indicate protein synthesis sites in presynaptic boutons. Scale bars = 1 and 0.2 μm, for dendrite and synapse, respectively. (**B-C**) Plots indicating frequency of nascent protein immunogold labeling in dendritic spines (**B**) and presynaptic boutons. * Kruskal-Wallis nonparametric test followed by Dunn's multiple comparison test, $p \leq 0.05$ (**C**). (**D**) Representative images of expanded cultured hippocampal neurons following 5 min of metabolic labelling and immunolabeling showing nascent protein detected in dendritic spines, excitatory presynaptic boutons or inhibitory presynaptic boutons. All scale bars = 5 μm. (**E**) Analysis of metabolic labeling showing that a large number of both pre- and postsynaptic compartments are translationally active within 5 min of metabolic labeling. *** Kruskal-Wallis nonparametric test followed by Dunn's multiple comparison test, $p \leq 0.001$. (**F-G**) Representative images showing newly synthesized proteins of interest, RapGEF4 and Bassoon, that were also identified as enriched in the vGLUT1+ transcriptome (Fig. 2G). Scale bar = 20 and 5 μm, for (F) and (G) respectively.

Fig. 4. Compartment-specific translation patterns decode different forms of plasticity.

(**A**) Scheme showing the timing of the different plasticity induction protocols and the metabolic labeling (+ puro). (**B**) Representative images showing both the immunostained, and metabolically labelled compartments indicating newly synthesized protein following expansion microscopy for one of the plasticity conditions (+/- BDNF). Scale bar = 5 μm. (**C**) Bar graphs indicating the specific translation pattern

in different subcellular compartments (vGAT+ or vGLUT1+ presynaptic terminals or spine) following the 3 different plasticity treatments, normalized to the control condition, n = 8-13 biological replicates per condition, for total puncta counted see numbers in the matrix shown in D. Unpaired t-tests, p values: ** $\leq$ 0.01, *** p $\leq$ 0.0001. (**D**) Matrix indicating both the synaptic compartment (spine, excitatory presynaptic compartment or inhibitory presynaptic compartment) and the plasticity agonist (BDNF, DHPG or ACEA) applied and the percentage of compartments that showed a metabolic label. In parentheses are shown the number of labeled compartments over the total number of compartments examined. Colors represent the change in protein synthesis- with green and lavender colors indicating a stimulation or repression of protein synthesis, respectively (see color look-up table). (**E**) Summary scheme indicating how each different form of plasticity examined has a specific translational signature. The 3 compartments represented by the horizontal boxes indicate the stimulation of protein synthesis by DHPG, BDNF, or ACEA, in that order.

Figure 1

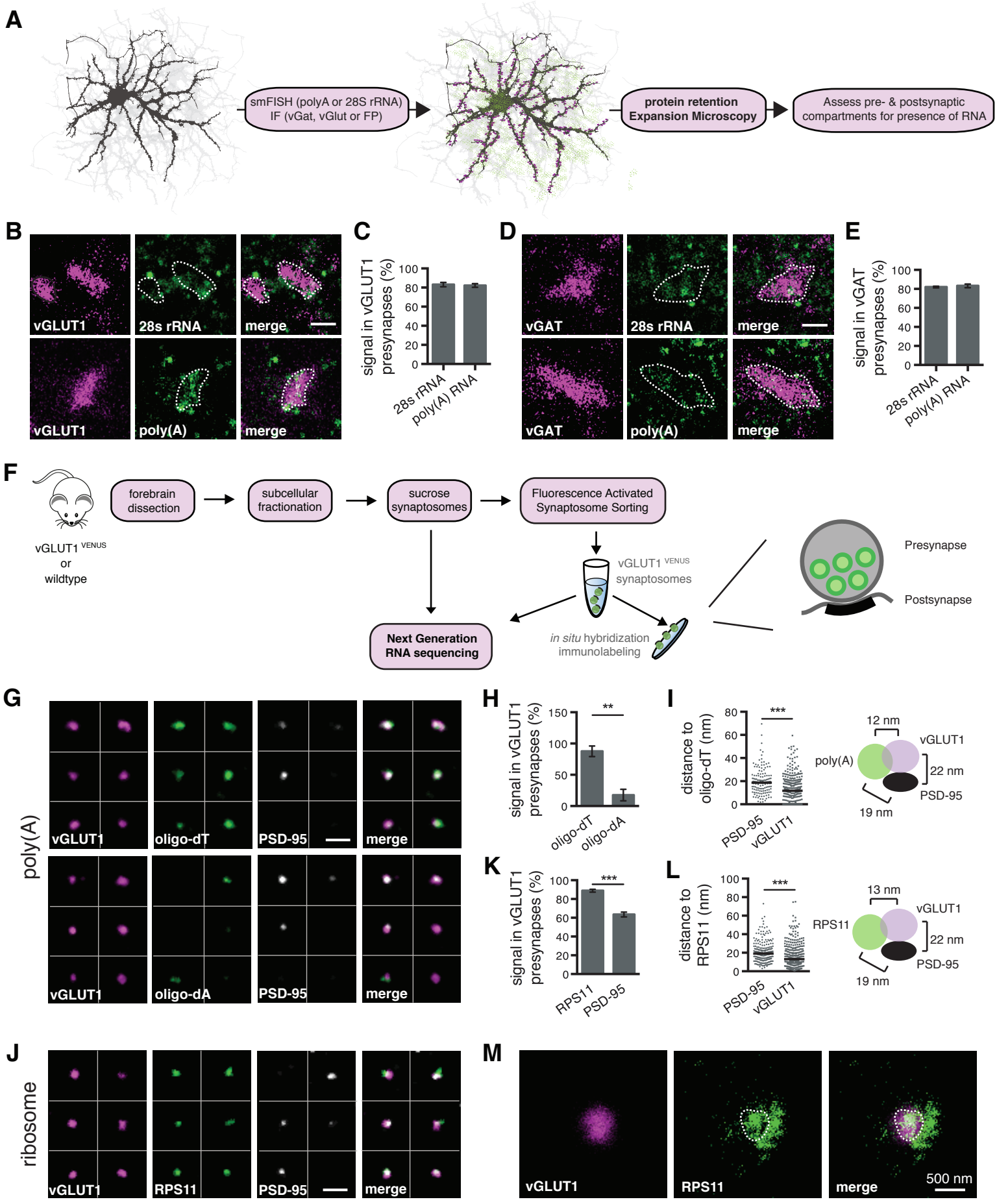
A
smFISH (polyA or 28S rRNA)
IF (vGat, vGlut or FP)
protein retention
Expansion Microscopy
Assess pre- & postsynaptic
compartments for presence of RNA
B
vGLUT1
28s rRNA
merge
vGLUT1
poly(A)
merge
C
signal in vGLUT1 presynapses (%)
100
80
60
40
20
0
28s rRNA
poly(A) RNA
D
vGAT
28s rRNA
merge
vGAT
poly(A)
merge
E
signal in vGAT presynapses (%)
100
80
60
40
20
0
28s rRNA
poly(A) RNA
F
vGLUT1 VENUS
or
wildtype
forebrain dissection
subcellular fractionation
sucrose synaptosomes
Fluorescence Activated Synaptosome Sorting
vGLUT1 VENUS synaptosomes
Next Generation RNA sequencing
in situ hybridization immunolabeling
Presynapse
Postsynapse
G
poly(A)
vGLUT1
oligo-dT
PSD-95
merge
vGLUT1
oligo-dA
PSD-95
merge
H
signal in vGLUT1 presynapses (%)
150
100
50
0
**
oligo-dT
oligo-dA
I
distance to oligo-dT (nm)
80
60
40
20
0
***
PSD-95
vGLUT1
poly(A)
12 nm
vGLUT1
22 nm
PSD-95
19 nm
K
signal in vGLUT1 presynapses (%)
100
80
60
40
20
0
***
RPS11
PSD-95
L
distance to RPS11 (nm)
100
80
60
40
20
0
***
PSD-95
vGLUT1
RPS11
13 nm
vGLUT1
22 nm
PSD-95
19 nm
J
ribosome
vGLUT1
RPS11
PSD-95
merge
M
vGLUT1
RPS11
merge
500 nm

Figure 2

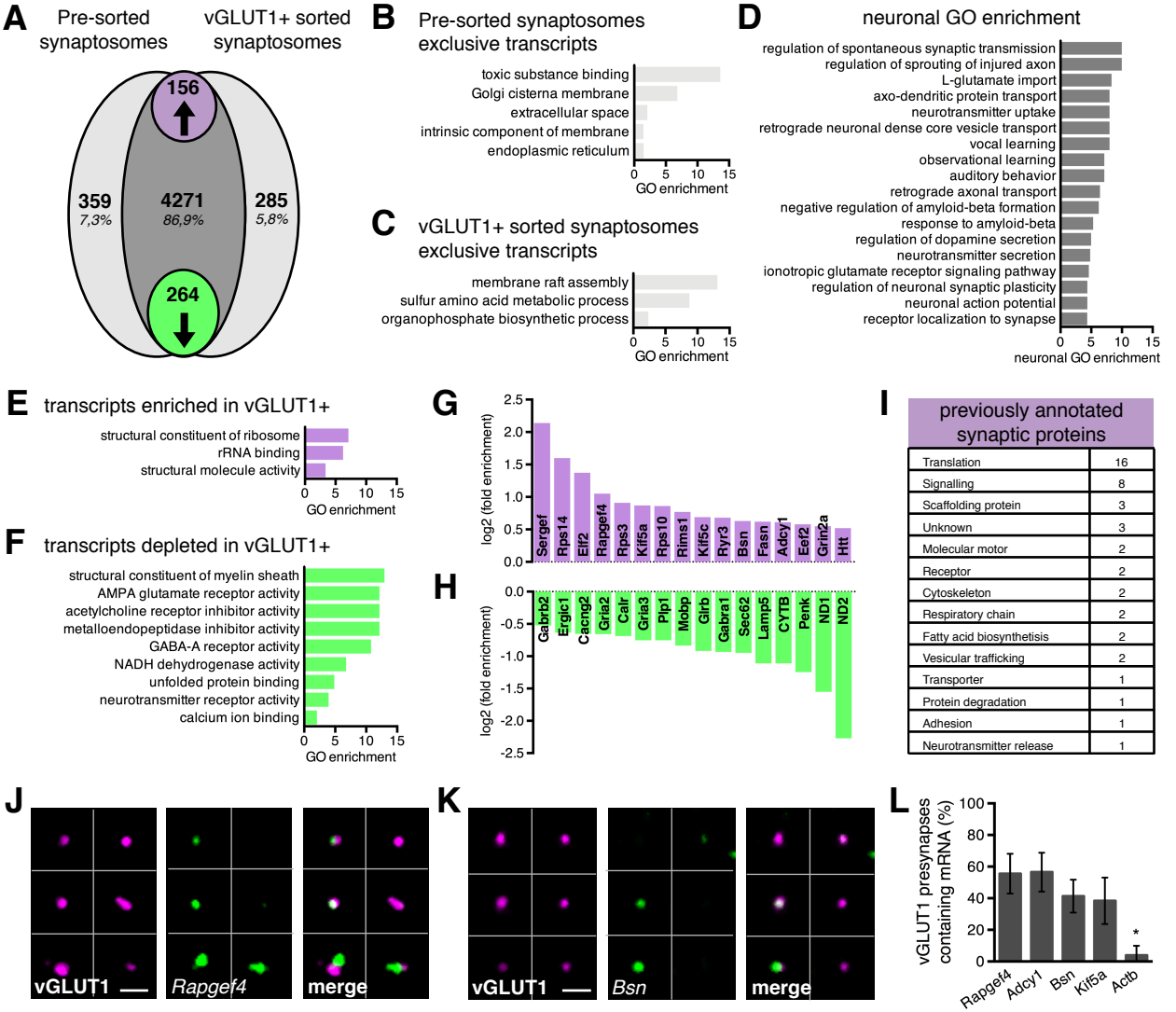
A
Pre-sorted synaptosomes
vGLUT1+ sorted synaptosomes
156
359
7,3%
4271
86,9%
285
5,8%
264
B
Pre-sorted synaptosomes exclusive transcripts
toxic substance binding
Golgi cisterna membrane
extracellular space
intrinsic component of membrane
endoplasmic reticulum
0 5 10 15
GO enrichment
C
vGLUT1+ sorted synaptosomes exclusive transcripts
membrane raft assembly
sulfur amino acid metabolic process
organophosphate biosynthetic process
0 5 10 15
GO enrichment
D
neuronal GO enrichment
regulation of spontaneous synaptic transmission
regulation of sprouting of injured axon
L-glutamate import
axo-dendritic protein transport
neurotransmitter uptake
retrograde neuronal dense core vesicle transport
vocal learning
observational learning
auditory behavior
retrograde axonal transport
negative regulation of amyloid-beta formation
response to amyloid-beta
regulation of dopamine secretion
neurotransmitter secretion
ionotropic glutamate receptor signaling pathway
regulation of neuronal synaptic plasticity
neuronal action potential
receptor localization to synapse
0 5 10 15
neuronal GO enrichment
E
transcripts enriched in vGLUT1+
structural constituent of ribosome
rRNA binding
structural molecule activity
0 5 10 15
GO enrichment
F
transcripts depleted in vGLUT1+
structural constituent of myelin sheath
AMPA glutamate receptor activity
acetylcholine receptor inhibitor activity
metalloendopeptidase inhibitor activity
GABA-A receptor activity
NADH dehydrogenase activity
unfolded protein binding
neurotransmitter receptor activity
calcium ion binding
0 5 10 15
GO enrichment
G
log2 (fold enrichment)
2.5 2.0 1.5 1.0 0.5 0.0
Sergef Rps14 Eif2 Rapgef4 Rps3 Kif5a Rps10 Rims1 Kif5c Ryr3 Bsn Fasn Adcy1 Eef2 Grin2a Htt
H
log2 (fold enrichment)
0.0 -0.5 -1.0 -1.5 -2.0 -2.5
Gabrb2 Erglc1 Cacng2 Gria2 Calr Gria3 Plp1 Mobp Girb Gabra1 Sec62 Lamp5 CYTB Penk ND1 ND2
I
previously annotated synaptic proteins
Translation 16
Signalling 8
Scaffolding protein 3
Unknown 3
Molecular motor 2
Receptor 2
Cytoskeleton 2
Respiratory chain 2
Fatty acid biosynthetisis 2
Vesicular trafficking 2
Transporter 1
Protein degradation 1
Adhesion 1
Neurotransmitter release 1
J
vGLUT1
Rapgef4
merge
K
vGLUT1
Bsn
merge
L
vGLUT1 presynapses containing mRNA (%)
100 80 60 40 20 0
*
Rapgef4 Adcy1 Bsn Kif5a Actb

Figure 3

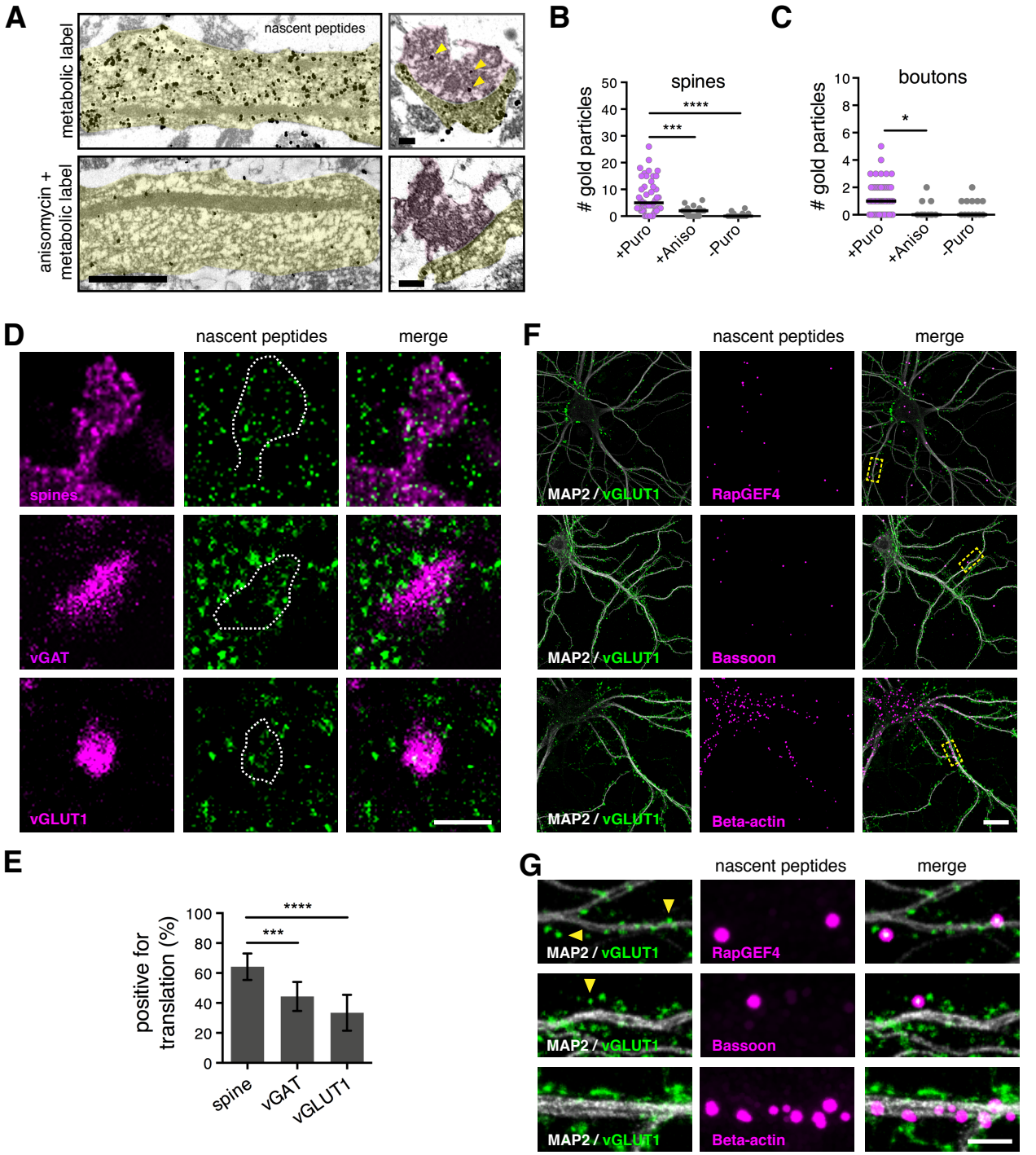
A
metabolic label
anisomycin + metabolic label
nascent peptides
B
spines
gold particles
50
40
30
20
10
0
****
***
+Puro
+Aniso
-Puro
C
boutons
gold particles
10
8
6
4
2
0
*
+Puro
+Aniso
-Puro
D
nascent peptides
merge
spines
vGAT
vGLUT1
F
nascent peptides
merge
MAP2 / vGLUT1
RapGEF4
Bassoon
Beta-actin
E
positive for translation (%)
100
80
60
40
20
0
****
***
spine
vGAT
vGLUT1
G
nascent peptides
merge
MAP2 / vGLUT1
RapGEF4
Bassoon
Beta-actin

Figure 4

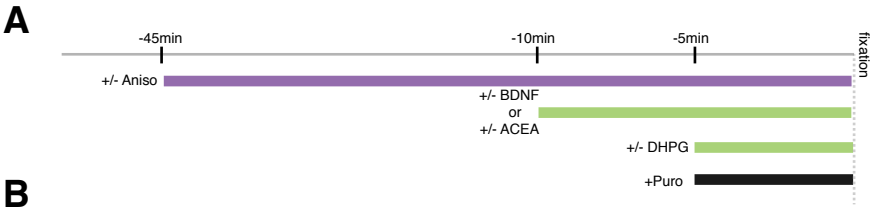

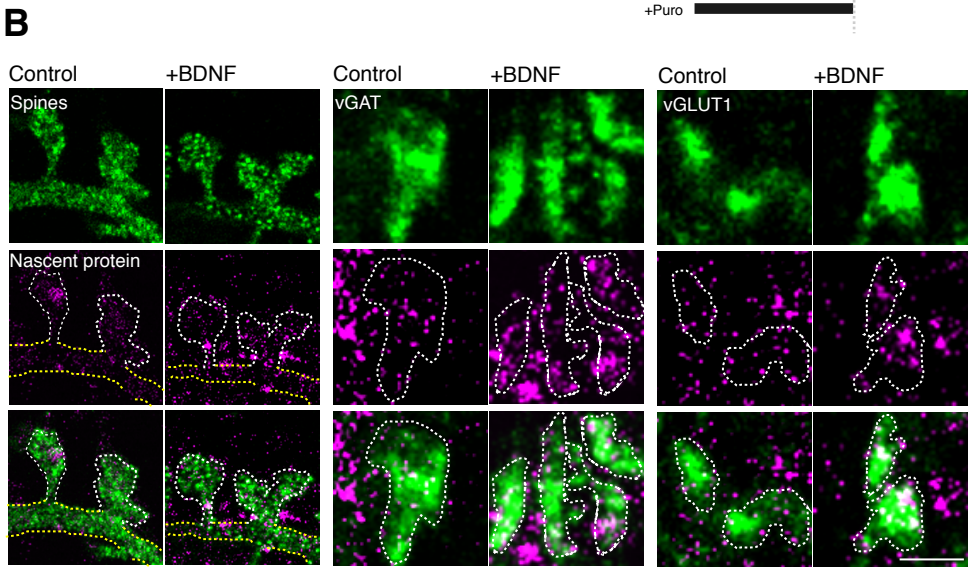

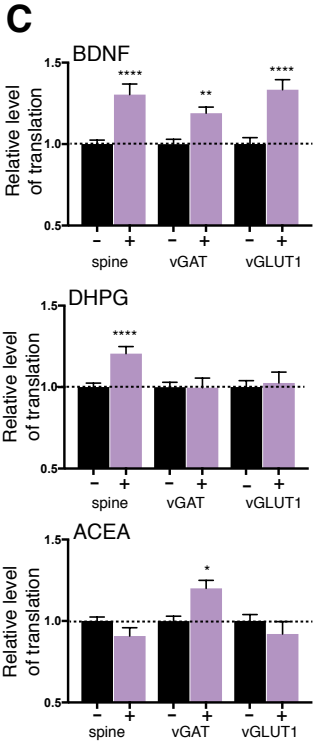

D

Compartment translational status

repressed — enhanced
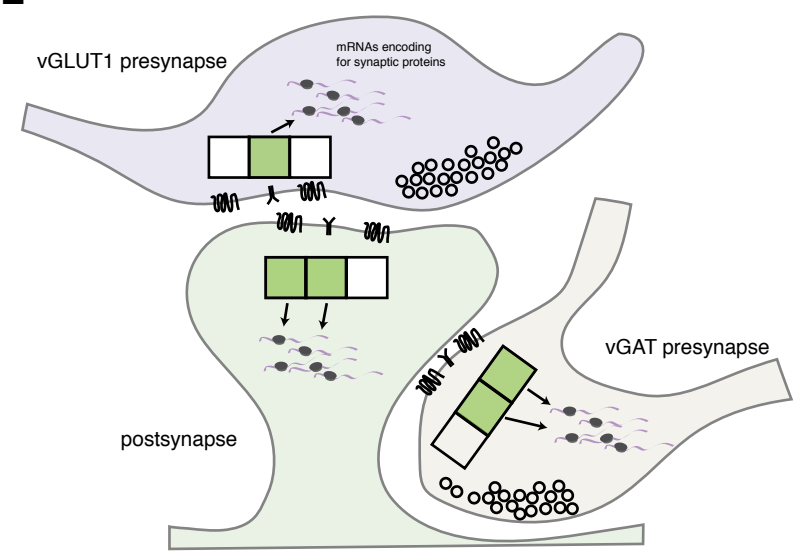
	spines	vGAT	vGLUT1
Control	60.8% (1852/3045)	44.2% (1693/3830)	36.5% (1208/3302)
+DHPG	74.4% (915/1231)	44.4% (630/1421)	37.1% (417/1123)
+BDNF	80.4% (1208/3302)	52.9% (742/1402)	48.3% (583/1206)
+ACEA	49.7% (602/1210)	53.4% (664/1242)	33.3% (391/1173)
+Aniso	14.3% (413/2892)	13.9% (528/3797)	13.3% (392/2940)